Catalysis Today 450 (2025) 115211

Contents lists available at ScienceDirect

Catalysis Today

journal homepage: www.elsevier.com/locate/cattod

Zr-modified USY zeolite as an efficient catalyst for the production of bio-jet fuel precursors from levulinic acid and furfural in the absence of solvent

Natalia Uricochea [a], Victor Uzquiano [a], Marta Paniagua [a], Gabriel Morales [a,b], Juan A. Melero [a,b,*]

[a] Chemical and Environmental Engineering Group. ESCET, Universidad Rey Juan Carlos. c/Tulipán s/n, Móstoles 28933, Spain
[b] Instituto de Investigación de Tecnologías para la Sostenibilidad (ITPS). ESCET, Universidad Rey Juan Carlos. c/Tulipán s/n, Móstoles 28933, Spain

ARTICLE INFO

Keywords:
Sustainable Aviation Fuel
Furfural
Levulinic Acid
Zeolites
Aldol Condensation

ABSTRACT

The high potential of using levulinic acid and furfural as platform molecules for the production of oxygenated adducts suitable as precursors for SAF synthesis is studied through the aldol condensation of both molecules. The research is the first-time demonstration of solventless acid-catalysed levulinic acid/furfural aldol condensation. The catalytic performance of a commercial H-USY zeolite and two post-synthetic variations thereof, with different dealumination degree and Zr loading, is analyzed, aiming at tuning the acid catalytic properties. The catalyst with an almost complete Al removal accompanied by the highest Zr wt% (Zr-USY-2) gave the best results in terms of selective conversion of furfural, pointing out to the Lewis acid sites as the main active sites to promote the aldol condensation reaction. An experimental design allowed to identify the optimal LA/FAL molar ratio (9/1) and reaction temperature (140 °C), while catalyst loading presented a minor significance. The optimization of the reaction parameters allowed to achieve a maximum furfural conversion of 88 %, combined with a yield towards the desired C10 adducts of 55 %. Furthermore, despite the catalytic performance of this material is slightly impaired in consecutive reaction cycles, it can be recovered with a thermal regeneration step, indicating a good reusability.

1. Introduction

Air transportation currently relies on fossil fuels, facing numerous challenges in the short term, not only because of the depletion of oil reserves but also because of accelerating decarbonization goals, as air traffic alone contributes today to roughly 2.5 % of the total global CO_2 emissions [1,2]. To tackle this challenge, many technology and research efforts are being devoted to finding alternative sources for synthesizing the so-called sustainable aviation fuels (SAFs) [3]. SAFs are already a viable alternative as they necessitate minimal to zero modifications in existing aircrafts for their utilization. However, there are still numerous challenges to address in the road to a final competitive commercial implementation, like SAFs manufacturing costs, production scalability, or the availability and affordability of the necessary raw materials.

A particularly promising solution due to its high availability are the so-called second-generation biomass feedstocks, which come from non-edible sources and therefore do not compete with food sector, like the exploitation of residual lignocellulosic biomass [4,5]. Among the potential biomass-converting technologies, the catalytic conversion of lignocellulosic platform molecules, like furfural and levulinic acid, emerges as a suitable alternative. These compounds already have mature industrial processes for their production. Levulinic acid (LA) is regarded as one of the most important building-block chemicals derived from biomass, which can be efficiently and economically produced from cellulosic materials through a commercial-scale acid-catalyzed hydrolysis process [6,7]. In turn, furfural (FAL) is already commercialized from the dehydration of xylose-rich materials, finding use as industrial solvent, as well as precursor for manufacturing an extensive number of chemicals and oxygenated and drop-in biofuels [8,9]. However, since these platform molecules have only 5–6 carbon atoms, to produce jet-fuel range products it is mandatory to enlarge the carbon backbone via C-C coupling reactions (e.g., aldol condensation, hydroxy-alkylation, ketonization, oligomerization, etc.). Subsequently, a hydro-deoxygenation process (HDO) is needed to remove the oxygenated moieties from the resultant aldol adducts, thus producing C_9-C_{14} hydrocarbons fully compatible with commercial kerosene [10].

* Corresponding author at: Chemical and Environmental Engineering Group. ESCET, Universidad Rey Juan Carlos. c/Tulipán s/n, Móstoles 28933, Spain.
E-mail address: juan.melero@urjc.es (J.A. Melero).

https://doi.org/10.1016/j.cattod.2025.115211
Received 3 December 2024; Received in revised form 9 January 2025; Accepted 20 January 2025
Available online 23 January 2025
0920-5861/© 2025 The Authors. Published by Elsevier B.V. This is an open access article under the CC BY-NC license (http://creativecommons.org/licenses/by-nc/4.0/).

One of the potential routes to produce SAFs starting from biomass-derived platform molecules is the cross condensation between LA and FAL, that can be catalyzed using a variety of materials. These include both homogeneous and heterogeneous catalysts, with basic and acidic reaction mechanisms [11]. The products coming from the C-C coupling reactions are mainly two furfurylidene-levulinic acid isomers having 10 carbon atoms (β-C10 and δ-C10). In the base catalysis route [12–15], despite milder reaction conditions can be used [16], the use of strong bases like NaOH implies significant technical challenges related to its corrosiveness and environmental impact, and to the control of the formation of undesired heavier condensation adducts, which are either too large for jet-fuel application or more difficult to manage [14]. As a way to overcome these drawbacks, the acid-catalyzed route has been recently explored, in special using acid zeolites (Y, beta, mordenite, ZSM-5) [17], as such or modified with enhanced porosity [13]. Also, other acid solid catalysts, like cation exchange resins and γ-Al_2O_3 have been tested with good results. Brønsted and Lewis acid sites can both contribute to the activity, and an adequate balance between them leads to enhanced selectivities[18].

The proposed experimental procedure to perform the aldol condensation in aqueous phase of FAL and LA previously reported in literature [11–15,17], involves a prior neutralization of the carboxylic group in LA with an inorganic salt, such as Na_2CO_3, to obtain the corresponding levulinate, which entails the need to carry out a final neutralization reaction with HCl after aldol condensation reaction to obtain the precursors of aviation compounds. This procedure decreases the sustainability of the process, with a high level of wastes generated, not being the most suitable at an industrial scale.

In this work we report for the first time the solventless acid-catalyzed condensation of LA and FAL avoiding pre-neutralization of the levulinic acid. In this way, several benefits are achieved: (1) more sustainable and eco-friendly process since the generation of hazardous waste and environmental pollution is reduced; (2) simplification of the process without the need to handle and separate a solvent, which can increase process efficiency and intensification; (3) cost reduction due to the reduction of operational and waste management costs. Moreover, as the nature and concentration of acid sites appear as critical for the catalytic performance, this work explores tuning the acidity of H-USY zeolite by selectively removing Al and introducing Zr sites on the zeolitic structure [19], in order to modulate the Brønsted/Lewis ratio of acid sites. The different nature of acid sites is shown as a key aspect for the promotion of aldol condensation reaction over undesired side reactions, leading to increased selectivities to the desired products.

2. Experimental

2.1. Materials

Levulinic acid (LA, 98 %, Sigma-Aldrich) and furfural (FAL, 99 %, Sigma-Aldrich) were used as reagents in the aldol condensation reaction. n-Decane (99 +%, Thermo Scientific) was used as internal standard, and ethyl acetate (>99.5 %, Sigma-Aldrich) as analytical solvent. Commercial H-USY zeolite (Zeolyst, CBV712) was used as starting material. Zirconium (IV) oxide in monoclinic phase (99 %, Sigma-Aldrich) was used as a commercial comparison catalyst. Nitric acid (HNO_3) (65 wt%, Sigma-Aldrich) was used in the dealumination process, and zirconium (IV) nitrate $Zr(NO_3)_4$ (98 +%, Chemicalpoint) was employed as Zr precursor.

2.2. Catalysts preparation

Two zirconium-modified USY zeolites were synthesized following the previously reported procedure. The commercial H-USY zeolite was subjected to dealumination using different concentrations of nitric acid (2 M and 10 M, 20 mL/g), contact times (1 h and 24 h), and temperatures (RT and 100 °C). The dealuminated zeolites were washed with deionized water, centrifugated to recover the solid sample, and dried overnight (110 °C). Afterwards, Zr was introduced via wet impregnation in water using the appropriate amount (equivalent to extracted aluminum) of Zr $(NO_3)_4$. Water was removed under vacuum from the resultant slurry and the solid was dried overnight and calcined in air following a 2-steps calcination: 200 °C for 6 h, and 550 °C for 6 h (3 °C/min heating ramp for both steps). This two-step calcination procedure allows for an adequate incorporation of the Zr species. The resultant Zr-modified USY catalysts are denoted as Zr-USY-1 for the milder dealumination conditions and Zr-USY-2 for the harsher ones.

2.3. Catalysts characterization

The techniques employed for the characterization of the commercial H-USY zeolite and the zirconium-modified USY zeolites synthesized are described below. Zr and Al loading were determined by Inductively Coupled Plasma-Optical Emission Spectroscopy (ICP-OES) using a Varian Vista AX apparatus. The Al speciation was analyzed by solid-state ^{27}Al MAS NMR on a Bruker Advance III/HD 400 spectrometer. To determine the crystallinity of the samples, powder X-ray diffraction (XRD) was used in a Philips X'pert diffractometer using the Cu Kα line in the 2θ angle range from 5° to 60° (step size of 0.04°). Structural characterization was completed by means of transmission electron microscopy (TEM) on a Philips Tecnai-20 electronic microscope operating at 200 kV. Textural properties were calculated from argon adsorption/desorption isotherms, which were recorded at 87 K using an AutoSorb equipment (Quantachrome Instruments). Average pore size was estimated using the NLDFT method, and total pore volume was taken at $P/P_o = 0.98$. *t*-plot method was used for the calculation of external surface and micropores areas. Acid capacity and strength were determined by temperature-programmed desorption of ammonia (NH_3-TPD) using an Autochem 2930 unit coupled to a TCD detector. X-ray Photoelectron Spectroscopy (XPS) measurements were obtained using a Specs Phoibos 150 9MCD photoelectron spectrometer. FTIR measurements for diffuse reflectance infrared Fourier Transform (DRIFT) were conducted using a Nicolet 5700 spectrometer equipped with an Hg-Cd-Te cryodetector. Pyridine served as a molecular probe to assess surface acidity, and the spectra were acquired in a reaction chamber equipped with a temperature controller, enabling in situ thermal treatments (Harrick Scientific Products, NY), and utilizing a praying mantis as a mirror optical accessory. Prior to recording the DRIFT spectra, the materials were treated at 120 °C for 1 h under an argon flow (50 mL min^{-1}) to clean the surface. Afterwards, a pyridine-saturated argon flow was passed through the sample until saturation. Physisorbed molecules were then removed by heating at 100 °C for 5 min and 120 °C for 1 h, again under Ar flow. DRIFT spectra were obtained in the spectral range of 4000–650 cm^{-1} with a resolution of 4 cm^{-1} after cooling the samples to room temperature. Brønsted to Lewis acid sites ratios were calculated assuming extinction coefficients previously reported in literature for zeolites. Thus, for the Py chemisorbed on Lewis acid sites (wavenumber 1446 cm^{-1}), 1.71 cm μmol^{-1} was used as the molar absorption coefficient. In turn, for the Py chemisorbed on Brønsted sites (1548 cm^{-1}), molar absorption coefficient was fixed at 1.54 cm μmol^{-1} [20].

2.4. Reaction procedure

Catalytic runs were performed to investigate the effect of different reaction conditions on the solventless aldol condensation of furfural (FAL) and levulinic acid (LA). The reactions were carried out in a carousel 12 Plus Reaction Station (Radleys) fitted with glass reactors (20 mL) and a stirring hotplate to control the reaction temperature and the magnetic agitation (400 rpm). In a typical assay, the catalyst is first introduced in the glass reactor, and then LA and FAL are added in the corresponding amounts. The reactor is then sealed and placed into the carousel. Upon completion, n-decane is added to the reaction content as internal standard to enable quantification of reactants conversion and

products yields. Typically, the composition of the reaction mixture was 0.48 g of FAL. Reaction conditions for the catalyst screening were fixed as follows: LA/FAL = 5 (mol/mol), FAL/Cat = 5 (wt./wt.), reaction temperature 120 °C, and reaction time 2 h. For the optimization of reaction conditions, reaction time was fixed at 2 h and the reaction variables investigated through a multivariable analysis were temperature (T = 100 – 120 – 140 °C), medium composition (LA/FAL molar ratio = 1 – 5 – 9), and catalyst loading referred to furfural (FAL/Cat mass ratio = 2.5 – 5 – 7.5). Under the optimized reaction conditions, the effect of reaction time was analysed in the range 0–6 h. Reusability experiments were performed after simple filtration and acetone washing at RT to remove remaining reaction media from catalyst surface. The resultant recovered material was then dried at 110 °C and used in a new otherwise equivalent reaction run.

2.5. Products analysis

Scheme 1 is a representation of the aldol condensation of furfural and levulinic acid, showing the two aldol products β- and δ-furfurylidenelevulinic acid (β-C10 and δ-C10). Chemical compounds identified by GC-Ms (Agilent 8860 GC System, HP-5MS column) included unreacted FAL and LA, n-decane used as internal standard, and the condensation products coming from the reaction of one molecule of FAL with one molecule of LA, herein denoted as β-C10 and δ-C10 (Scheme 1). It is important to note that each product, the branched β-C10 and the linear δ-C10 can include two isomers (cis and trans) [17], which have been quantified together. Some other compounds, attributed to the self-aldol condensation of levulinic acid and the condensation of two molecules of FAL with a molecule of LA [14], have not been detected under the tested reaction conditions.

Reaction samples were analyzed by means of gas chromatography (Agilent Intuvo 9000 chromatograph) using a 30 m long Agilent DB-5 column and a flame ionization detector (FID). Products quantification was obtained by GC calculating the corresponding response factors: standard stock solutions were used for commercially available FAL and LA, and the effective carbon number concept was used for the quantification of non-commercially available C10 condensation products [21]. Catalytic results were defined in terms of conversion of furfural (X_{FAL}) as the limiting reactant, and yield (Y_{C10})/selectivity (S_{C10}) to the desired condensation products (C10):

$$X_{FAL}\ (\%) = \frac{(\text{initial mmol of furfural}) - (\text{final mmol of furfural})}{\text{initial mmol of furfural}} \text{x}100 \quad (1)$$

$$Y_{C10}\ (\%) = \frac{\text{mmol of product C10}}{\text{initial mmol of furfural}} \text{x}100 \quad (2)$$

$$S_{C10}\ (\%) = \frac{Y_{C10}}{X_{FAL}} \text{x}100 \quad (3)$$

3. Results and discussion

3.1. Catalysts characterization

Two catalysts with different Zr/(Zr+Al) ratio were synthesized modifying the parent H-USY zeolite via dealumination and subsequent Zr incorporation. Table 1 includes the most relevant physicochemical properties of these materials, including the parent H-USY zeolite for comparison. The dealumination treatment with 2 M HNO_3 led to the removal of approximately 76 % of the Al content (Zr-USY-1). More stringent dealumination conditions (10 M HNO_3, 24 h, 100 °C) gave a higher dealumination degree of 88 % (Zr-USY-2), but could not reach a total Al removal. This reveals the challenge of fully extracting Al from the FAU lattice without impairing the crystalline structure. The Zr-modified materials present varying Si/Al ratios (31.6–61.1) and Zr loadings (8.9–10.9 wt%).

Fig. 1 shows the characterization of commercial and Zr-modified USY zeolites. Fig. 1a includes the XRD patterns of the prepared materials, the parent H-USY and the crystalline ZrO_2, confirming the preservation of the crystallinity in the modified zeolites. Moreover, no evidence of diffractions characteristic of zirconia is observed for these samples, indicating a good dispersion of Zr onto the Al vacancies generated by dealumination. TEM analysis also confirms the preservation of the microporous structure integrity, with a minor distortion effect on the surface, as inferred from the image blurring in the modified material Zr-USY-1 (Fig. S1). Furthermore, regarding Zr speciation, TEM micrographs do not show any evidence of ZrO_2 bulk agglomerates, in consonance with the results from DRX, and indicating a lattice incorporation of the Zr species, most likely on the hydroxyl nests generated during the dealumination process. As further evidence of the incorporation of Zr into the generated Al vacancies, Zr XPS analysis was also performed (Fig. S2). XPS spectra reveal a shift of the Zr 3d signals to lower binding energies, closer to the signal attributed to ZrO_2, as the Zr content increases, suggesting a different environment in Zr-USY materials in comparison with pure crystalline ZrO_2.

Regarding textural properties, measured by argon adsorption-desorption (Fig. 1b and Fig. S3), the resultant isotherms correspond to microporous materials. However, a small hysteresis loop can be observed (already present in the parent H-USY material) and indicating a small proportion of mesoporosity, probably coming from the synthetic procedure of stabilization of the original Y zeolite to obtain USY version. In the modified materials, the dealumination and subsequent Zr incorporation produce an increase of the external surface area (S_{EXT}, from 80 to 145 m^2/g), as well as of the total pore volume (from 0.39 to 0.46 cm^3/g), which is attributed to the introduction of a higher proportion of defects during Al removal by acid treatment. However, as evidenced by the XRD diffractograms (Fig. 1a), such defects do not significantly alter the FAU crystalline structure.

Likewise, the solid-state ^{27}Al NMR analysis (Fig. 1c) demonstrates that during the aluminum extraction the extra-framework octahedrally coordinated Al is more easily removed (0 ppm chemical shift) as compared to the lattice tetrahedrally coordinated Al (approx. 55 ppm chemical shift). Interestingly, for the highly dealuminated sample, Zr-USY-2, no Al signals can be detected, reflecting the very low Al content of this sample and confirming the efficiency of the dealumination process under the more stringent conditions. Regarding the acid properties, the NH_3-TPD analysis unmasks both the number and the strength of acid centers (Fig. 1d). Thus, TPD signal decreases insofar as the Zr loading increases, and the maximum desorption peak is shifted to lower temperatures (T_{max}, Table 1). This indicates not only a reduction in the

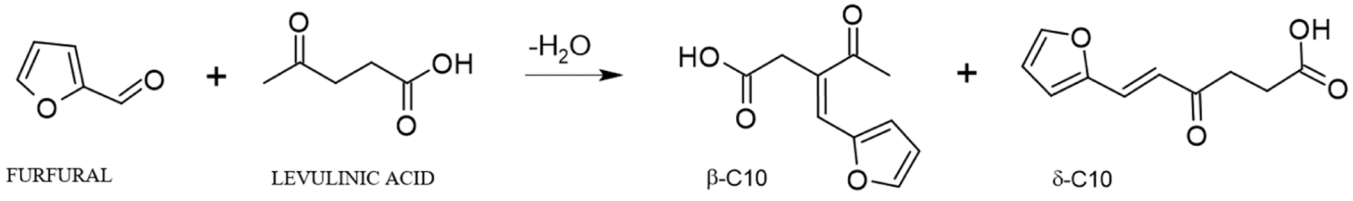

Scheme 1. Simplified reaction scheme for the aldol condensation of FAL and LA, including the main furfurylidene-levulinic acid isomers obtained in the acid-catalyzed route.

Table 1
Physicochemical properties of parent and Zr-modified USY zeolites: composition, textural properties and acidity.

Catalyst	Composition				Textural properties			Acid properties		
	Al (wt%)	Zr (wt%)	Si/Al	Zr/(Zr+Al)	S_{BET} (m^2/g)[c]		V_p (cm^3/g)	Capacity[d] (mmol H^+/g)	T_{max}[e] (°C)	B/L ratio[f]
					S_{EXT}	$S_{\mu p}$				
H-USY	5.2	0	7.8	0	80	616	0.39	0.65	307	0.37
Zr-USY−1[a]	1.2	8.9	31.6	0.7	114	557	0.39	0.31	288	0.21
Zr-USY−2[b]	0.6	10.9	61.1	0.9	145	580	0.46	0.14	247	0.04

[a] Dealumination conditions: 2 M nitric acid, 1 h, RT;
[b] Dealumination conditions: 10 M nitric acid, 24 h, 100 °C;
[c] External surface area and micropores area calculated with the *t*-plot method;
[d] Total acid capacity determined using NH_3-TPD;
[e] Temperature of the maximum desorption of NH_3 analyzed by NH_3-TPD.
[f] Brønsted/Lewis acid sites ratio determined by FTIR using pyridine as molecular probe (meq/meq).

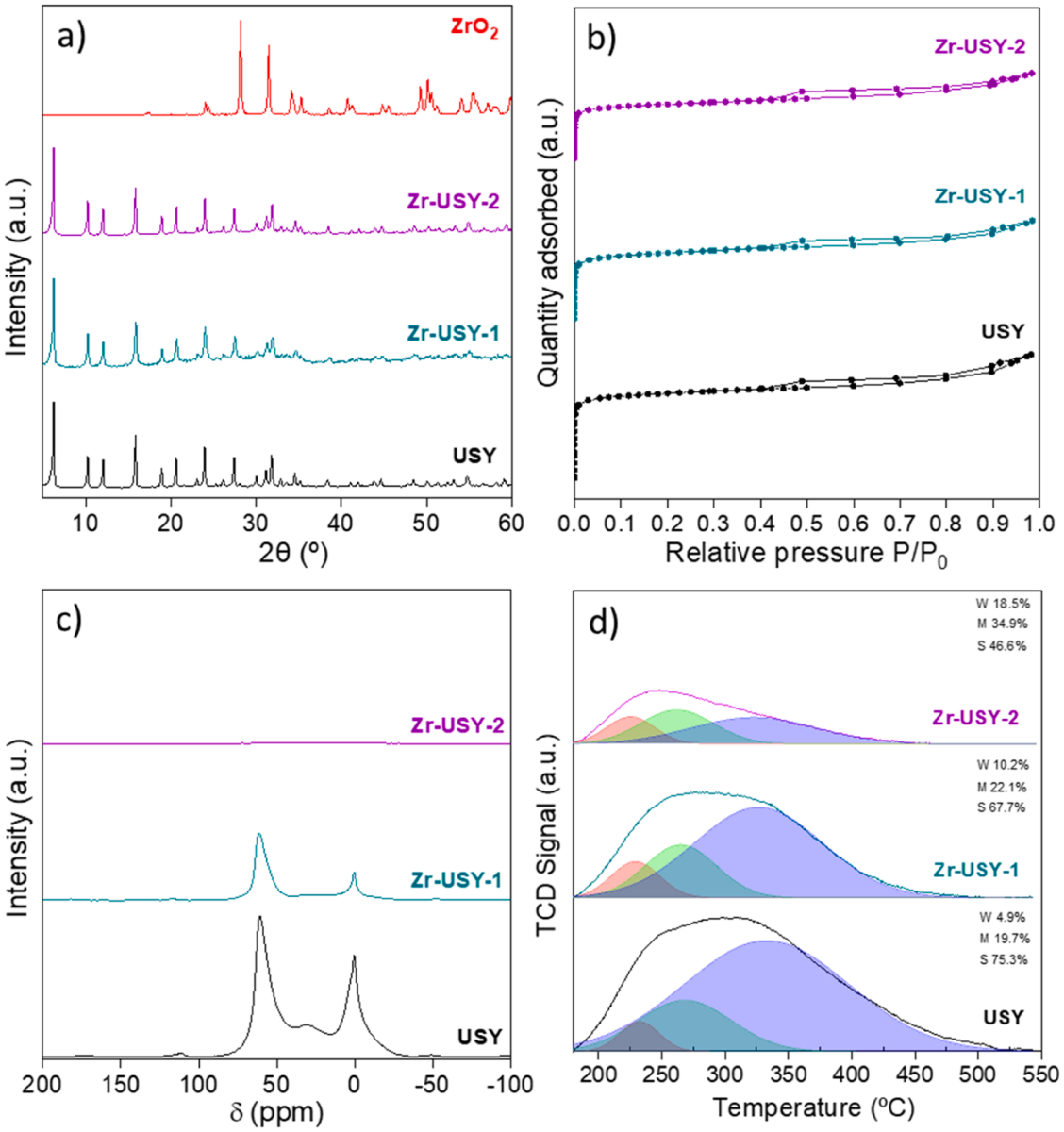

Fig. 1. Characterization of commercial and Zr-modified USY zeolites. a) Wide-angle XRD patterns; b) argon adsorption-desorption isotherms; c) solid-state ^{27}Al NMR spectra; d) NH_3-TPD analysis. W: weak, M: medium, S: strong acid sites.

overall available acidity but also a weaker character of such acidity, at least as inferred from the interaction with NH_3 molecules, more prone to interact with Brønsted rather than Lewis acid centers. On the other hand, to determine the Brønsted/Lewis acid sites ratio (B/L), pyridine FTIR experiments were conducted. The use of pyridine as a probe molecule allows distinguish between Brønsted and Lewis acid sites, as the infrared

spectra exhibit two absorption bands [22]. The parent H-USY zeolite displays both types of acid sites, as indicated by the presence of both signals: the one corresponding to Lewis acid sites around 1446 cm^{-1}, and the characteristic signal of Brønsted acid sites at 1548 cm^{-1} (Fig. S4). It is noted that the band for Brønsted sites is quite weak, being appreciable only in the commercial H-USY zeolite. As the aluminum content decreases, the signal in this band becomes less perceptible. Regarding the Lewis acidity signal, it is observed that the signal becomes more intense as the zirconium content in the Zr-USY material increases, with the most intense peak for the Zr-USY-2 material. The integration of the characteristic signals provides the values for the B/L ratio shown in Table 1. The quantification reflects that the substitution of Al with Zr in the zeolites results in the removal of Brønsted acid sites and the incorporation of Lewis acidity, thereby increasing the proportion of the latter and therefore decreasing the B/L ratio.

3.2. Catalytic screening of Zr-USY zeolites

The synthesized materials were evaluated in the aldol condensation of LA and FAL to observe the consequences of decreasing Al-derived acidity along with the impact of incorporating Zr. Commercial H-USY zeolite and commercial monoclinic zirconia ZrO_2 were used as reference catalysts. For this study, a molar ratio of LA/FAL = 5 was used, the catalyst amount was fixed to obtain a FAL/Cat mass ratio of 5, and the reaction temperature and time were set at 120 °C and 2 h. These screening conditions were chosen based on insights gained from previous investigations involving other zeolites [17]. Noteworthy, no additional solvent is used in the system, just furfural and levulinic acid. Fig. 2 illustrates the results from this catalysts screening. As a reaction control, a blank run in the absence of catalyst was carried out, giving low FAL conversion and a negligible amount of aldol condensation products. This indicates that, under the tested reaction conditions, the extent of the aldol condensation of FAL and LA via autocatalysis is insignificant. So the presence of an acid catalyst, at least one more active than levulinic acid itself, is necessary to drive this condensation reaction. In turn, commercial ZrO_2 has high crystallinity as seen in the XRD spectrum, a low specific surface area (less than 5 m^2/g) and according to the TPD results, it does not present acidity, at least not strong enough to interact with ammonia in the analysis conditions. The poor catalytic results obtained over this material can then be attributed to the fact that the Zr is fully coordinated in the form of oxide, with low porosity and surface defects, which renders it as not catalytically active in this reaction (slightly over the blank reaction).

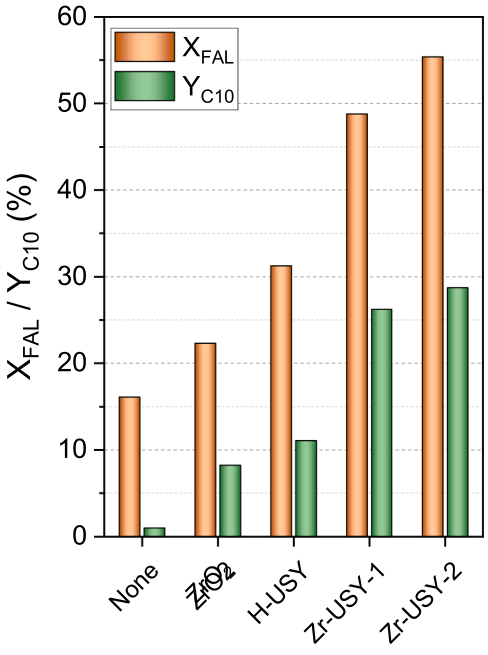

Fig. 2. Screening of commercial catalysts and Zr-USY modified zeolites in the aldol condensation of FAL and LA. Reaction conditions: LA/FAL = 5 (mol/mol), FAL/Cat = 5 (wt./wt.), T = 120 °C, t = 2 h.

Regarding the zeolitic materials, in terms of activity, a higher Zr loading in the FAU framework enhances FAL conversion, progressing from 31.3 % for H-USY to 55.4 % for Zr-USY-2. In terms of oxygenated adducts production, the lowest value of Y_{C10} corresponds to the unmodified parent zeolite, while for the Zr-modified versions, much better results are obtained. As determined in the previous section, the synthesized Zr-USY materials present two types of catalytic functionalities: Brønsted acid sites, which come from the compensation of protons in the tetrahedral aluminum atoms of the zeolitic structure, and Lewis acid sites that mainly come from the zirconium atoms isomorphically incorporated in lattice positions substituting the extracted aluminum species, as well as from remaining the extra-framework Al species. The catalytic results indicate that the aldol condensation of furfural with levulinic acid is benefited from the presence of highly dispersed Zr on the zeolitic framework, not only in the improvement of FAL conversion, but also on the promotion of aldol condensation pathway achieving higher yields of the desired C10 adducts. This transformation is probably being promoted by Lewis acid sites incorporated in the synthesized Zr-USY materials. Furthermore, the decrease in the Brønsted acidity after Al removal appears to minimize the undesired furfural polymerization reactions, leading to a better selectivity of the reaction.

Moreover, under these reaction conditions, the formation of the branched β-C10 isomer is favored over the production of the linear δ-C10 (Table S1). In the reaction mechanism of the acid-catalyzed aldol condensation, the favored intermediate enol is the one formed through the protonation of the carbonyl group of LA, after attack the carbonyl group of FAL, finally giving β-C10 product [11].

As a further demonstration of the effect of Zr sites in this system, partially dealuminated USY (dAl-USY-1) and almost totally dealuminated USY (dAl-USY-2) were also assessed in the aldol condensation of FAL and LA (Fig. S5). After partial dealumination of the H-USY zeolite, and before Zr incorporation, the catalytic activity is similar to the parent zeolite, indicating that the loss of acid sites during the dealumination process is compensated by the greater accessibility to the acid sites and by the higher proportion of extra-framework Al, corresponding to Lewis acid sites which are less active in converting furfural. However, when Al is almost totally extracted, a loss of catalytic activity both in terms of furfural conversion and yield to C10 adducts is observed, getting a very low selectivity to the desired products. These results corroborate that it is the presence of Zr that provides the improvement of the catalytic activity in the synthesized Zr-USY materials.

3.3. Optimization of reaction conditions

From the above catalyst screening, the difference between both Zr-modified samples is small, but the slightly higher C10 yield obtained over Zr-USY-2 catalyst determined its selection for a further optimization study. In this way, to enhance the catalytic performance of Zr-USY-2, an experimental design methodology was applied to optimize the reaction conditions with the objective of maximizing the conversion of FAL along with the production of the aldol condensation adducts. The selected experimental matrix features the three most influential variables in this system as reported in previous works [17,18], including temperature (T), LA/FAL molar ratio (MR), and catalyst loading expressed as FAL/Cat mass ratio (Cat). Moreover, due to the occurrence of side reactions, cross-interactions between variables can be expected. Therefore, in order to simultaneously study these three main factors at three different levels each, a full 3^3 factorial experimental design was implemented. The lower and upper level of the experimental factors were: 100 – 140 °C for the temperature, 1 – 9 for the LA/FAL molar ratio, and 2.5 – 7.5 for the FAL/Cat mass ratio. Table 2 outlines the complete

Table 2
Matrix of experiments and experimental results for the aldol condensation of FAL and LA over Zr-USY-2. Reaction time = 2 h.

Run	T (°C)	MR (mol/mol)	Cat (wt./wt.)	I_T	I_{MR}	I_{Cat}	X_{FAL} (%)	Y_{C10} (%)	S_{C10} (%)
1	100	1	7.5	−1	−1	1	24.5	3.5	14.1
2	100	1	5	−1	−1	0	26.7	5.9	21.9
3	100	1	2.5	−1	−1	−1	36.0	10.5	29.1
4	100	5	7.5	−1	0	1	20.0	5.7	28.6
5	100	5	5	−1	0	0	23.9	7.3	30.4
6	100	5	2.5	−1	0	−1	29.3	13.2	45.0
7	100	9	7.5	−1	1	1	17.1	3.7	21.5
8	100	9	5	−1	1	0	18.0	3.4	18.8
9	100	9	2.5	−1	1	−1	21.9	8.2	37.6
10	120	1	7.5	0	−1	1	36.0	12.7	35.3
11	120	1	5	0	−1	0	55.6	19.7	35.4
12	120	1	2.5	0	−1	−1	64.8	21.7	33.4
13	120	5	7.5	0	0	1	45.6	24.0	52.5
14	120	5	5	0	0	0	53.9	25.8	48.6
15	120	5	2.5	0	0	−1	66.3	36.7	55.4
16	120	9	7.5	0	1	1	45.3	22.9	52.2
17	120	9	5	0	1	0	65.7	19.7	30.0
18	120	9	2.5	0	1	−1	67.7	33.4	49.9
19	140	1	7.5	1	−1	1	89.5	1.1	1.3
20	140	1	5	1	−1	0	87.0	1.4	1.7
21	140	1	2.5	1	−1	−1	90.6	1.0	1.1
22	140	5	7.5	1	0	1	89.3	39.7	44.5
23	140	5	5	1	0	0	95.2	38.9	40.9
24	140	5	2.5	1	0	−1	97.7	37.8	38.7
25	140	9	7.5	1	1	1	88.2	55.4	62.8
26	140	9	5	1	1	0	84.2	51.6	61.2
27	140	9	2.5	1	1	−1	96.7	54.6	56.5
28	120	5	5	0	0	0	49.4	30.5	61.7
29	120	5	5	0	0	0	51.1	26.1	51.1
30	120	5	5	0	0	0	53.7	32.7	60.8

Note: I_T, coded value for temperature; I_{MR}, coded value for LA/FAL molar ratio; I_{Cat}, coded value for FAL/Cat mass ratio; X_{FAL}, conversion of FAL; Y_{C10}, yield to C10; S_{C10}, selectivity to C10.

experiments set, including the results obtained for the selected variables: conversion of FAL and yield/selectivity of C10 isomers. Experiments were conducted in a randomized manner to mitigate errors arising from potential systematic trends in the variables.

Each response factor has been fitted to a quadratic model, resulting in a mathematic model that combines the factors and their interactions in a coded format using a second-order polynomial equation:

$$Y = \beta_0 + \sum_{i=1}^{2} \beta_i \cdot X_i + \sum_{i=1}^{2} \beta_{ii} \cdot X_i^{\,2} + \sum_{i=1}^{2} \beta_{ij} \cdot X_i \cdot X_j$$

where Y is each response (FAL conversion, yield to C10, or selectivity to C10, mol%) and β_0, β_i, β_{ii} and β_{ij} are the regression coefficients of intercept, linear, quadratic and binary interactions, respectively. X_i and X_j are the independent factors, temperature, LA/FAL molar ratio, and FAL/Cat mass ratio. To validate the parameter estimation and ensure the accuracy of the model fitting, an estimation of the statistical error was conducted. Eqs. 1–3 were obtained through multiple regression analysis using the Statgraphics software, based on the matrix generated from the experimental data (Table 3). The statistical models are obtained from encoded levels giving the real influence of each variable on the process.

Table 3
Predictive model equations obtained by response surface methodology.

Statistical models	r^2	
$X_{FAL}(\%) = 54.31 + 33.51I_T - 0.45I_{MR} - 6.44I_{Cat} + 2.99I_T^2 + 2.48I_TI_{MR} + 0.60I_TI_{Cat} - 0.41I_{MR}^2 + 0.51I_{MR}I_{Cat} + 0.97I_{Cat}^2$	0.968	(1)
$Y_{C10}(\%) = 28.31 + 12.32I_T + 9.67I_{MR} - 2.59I_{Cat} - 5.40I_T^2 + 13.43I_TI_{MR} + 1.99I_TI_{Cat} - 7.50I_{MR}^2 - 0.04I_{MR}I_{Cat} + 1.82I_{Cat}^2$	0.931	(2)
$S_{C10}(\%) = 52.34 + 3.51I_T + 11.97I_{MR} - 1.76I_{Cat} - 14.53I_T^2 + 13.53I_TI_{MR} + 5.17I_TI_{Cat} - 13.17I_{MR}^2 + 0.28I_{MR}I_{Cat} + 2.89I_{Cat}^2$	0.889	(3)

Note: I_T, coded value for temperature; I_{MR}, coded value for LA/FAL molar ratio; I_{Cat}, coded value for FAL/Cat mass ratio; X_{FAL}, conversion of FAL; Y_{C10}, yield to C10; S_{C10}, selectivity to C10.

Hence, the resultant model equations can be used to facilitate visualization and comprehension of the optimization phenomena.

The relatively high regression coefficients obtained ensure the goodness of the fit. Fig. S6 depicts the correlation between experimental results (Table 2) and the corresponding predicted values obtained using the mathematical models (Table 3). For the FAL conversion there is an excellent agreement between experimental results and predicted values, while for the yield and selectivity to C10 a greater dispersion is observed. Additionally, the reproducibility of the experimental system was evaluated by performing four replicas of the central point experiment (120 °C, LA/FAL molar ratio = 5, FAL/Cat mass ratio = 5). The average values and their standard deviations were: FAL conversion 52.0 ± 2.2 %, C10 yield 28.8 ± 3.4 % and C10 selectivity 55.6 ± 6.6 %. Consequently, the obtained standard deviations are low enough to consider the experimental error as not very significant, especially for FAL conversion and yield to C10.

Additionally, Fig. 3 represents the model-generated response surfaces corresponding to X_{FAL}, graphically displaying the effect of LA/FAL and FAL/Cat ratios on both variables at a fixed reaction temperature. Based on the design of experiments, it is identified that the factor with the greatest impact on FAL conversion is the linear contribution of temperature, reaching almost a complete conversion at a temperature of 140 °C. This result indicates that an increase in the reaction temperature leads to the promotion of FAL conversion, but both in the aldol condensation and in the undesired side reactions. On the other hand, in general, the level of levulinic acid excess with respect to furfural is hardly relevant. Also, there is a reduced effect of the amount of catalyst present, particularly increasing the conversion at lower FAL/Cat ratios and vice versa. The rest of the effects, including the interactions between the factors, and the quadratic effect of them are not significant in the adjusted model, as evidenced by the roughly horizontal arrangement of the response surfaces (Fig. 3). Thus, from the point of view of furfural conversion, it would be necessary to work at the highest temperature (140 °C), LA/FAL molar ratio (9), and the lowest FAL/Cat mass ratio

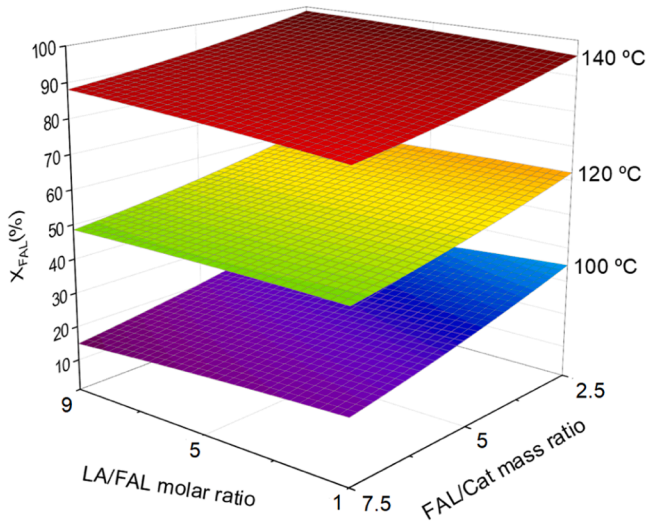

Fig. 3. Response surfaces corresponding to FAL conversion in the aldol condensation of FAL and LA over Zr-USY-2 predicted by the model at different temperatures.

(2.5), to reach the maximum FAL conversion of 98.7 %.

According to Eq. 2 corresponding to the yield to C10 (Table 3), visualized graphically in Fig. 4, various factors beyond the linear effect of temperature gain increased significance. Specifically, the interaction between temperature and LA/FAL molar ratio appears as the most important factor, with a significant positive influence on yield to C10. As shown in Fig. 4, at low temperature, an increase in LA/FAL molar ratio leads to a decrease in the formation of C10, while as the temperature reaches higher values, the effect of LA/FAL molar ratio becomes the opposite. The next factors in importance are the linear effect of temperature and LA/FAL molar ratio, with a positive effect on the yield to C10. In addition, the quadratic effect of LA/FAL molar ratio and temperature have also a significant negative influence, indicating that the increase in these factors does not produce a constant rise in the yield to C10, which can be attributed to a significant curvature effect at the lower levels of them. Thus, from the point of view of C10 yield, it is necessary to work at 140 °C and LA/FAL = 9, resulting in a maximum yield of C10 around 55 %.

Regarding the selectivity towards the aldol condensation product, Eq. 3 (Table 3) and Fig. 5, the significant factors are like those discussed for the yield to C10. Again, a significant curvature effect of temperature and LA/FAL molar ratio is observed at the lowest level thereof. The general trend in the design also suggests the use of an excess of levulinic acid as positive. As evidenced in Fig. 5, operating within the range of LA/FAL = 5–7 permits to work below 140 °C. Additionally, the low selectivity associated with high temperature and high FAL concentration is emphasized, making clear the presence of other undesired routes of furfural transformation. So, working at high temperatures and high LA/FAL molar ratios may represent the best choice, reaching selectivities close to 60 %.

In order to further study the effect of temperature, an additional experiment was performed at 160 °C, at the highest LA/FAL molar ratio. However, a pronounced drop in yield and selectivity to C10 was obtained, indicating that at such high temperatures, FAL degrades to undesired products and C10 adducts evolve via oligomerization to give heavier condensation products (not detectable by GC).

As a conclusion of this optimization study, it has been determined that the most significant factors in the aldol condensation of FAL and LA are the temperature and the LA/FAL molar ratio, while the amount of catalyst within the range studied is not a determining factor for any of the responses under study. Furthermore, a relevant curvature of the response surfaces has been observed for the effect of two significant variables (T and RM) in both the yield and the selectivity towards C10 products, as well as a strong interaction between them. Therefore, optimal operating conditions, in which the three response variables, FAL conversion, yield, and selectivity to C10, are maximized simultaneously, would be: T = 140 °C, LA/FAL = 9, and FAL/Cat = 7.5 ($I_T = +1$, $I_{MR} = +1$, $I_{Cat} = +1$ in coded values). Applying the mathematical models, in these reaction conditions the predicted values are: X_{FAL} = 88.1 %; Y_{C10} = 52 %; S_{C10} = 60.2 %. It must be also noted that, under these optimized conditions, the effect of reaction time is shown as critical in order to achieve maximum yield to aldol condensation products (Fig. S7). Thus, after reaching the maximum yield to C10 at around 2 h, it starts to decrease slowly insofar as the oligomerization of the formed aldol condensation products takes place [17].

3.4. Reusability of the catalyst

The reusability of Zr-USY-2 was explored by analyzing its catalytic performance in three consecutive reaction cycles, at 2 h and under the reaction conditions maximizing C10 yield (T = 140 °C, LA/FAL = 9, and FAL/Cat = 7.5). Catalyst was recovered in between uses by simple filtration, acetone washing and overnight drying at RT. Fig. 6a includes the catalytic results, evidencing a progressive but small deactivation of the catalyst, both in terms of FAL conversion and yield to desired products.

Spent catalysts from runs 2 and 3 were analyzed by means of thermogravimetric analysis, as depicted in Fig. 6b. The results evidence that catalyst deactivation is attributable to the deposition of organic compounds on the catalyst surface that could come from both the C10 condensation products and the FAL polymerization side reactions, considering that the selectivity remains approximately 60 % across all catalytic cycles. The spent catalyst after three catalytic cycles (run 3)

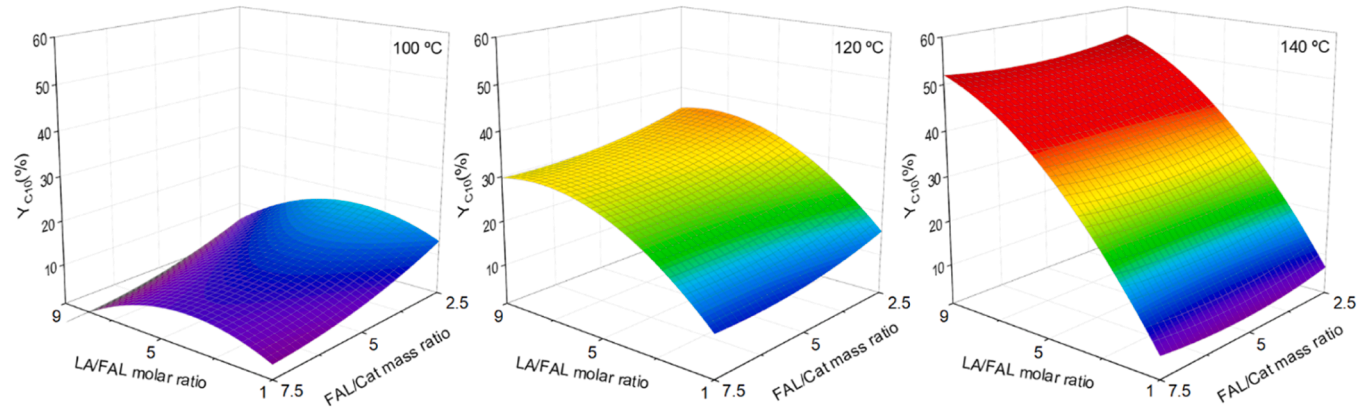

Fig. 4. Response surfaces corresponding to the yield to C10 in the aldol condensation of FAL and LA over Zr-USY-2 predicted by the model at different temperatures.

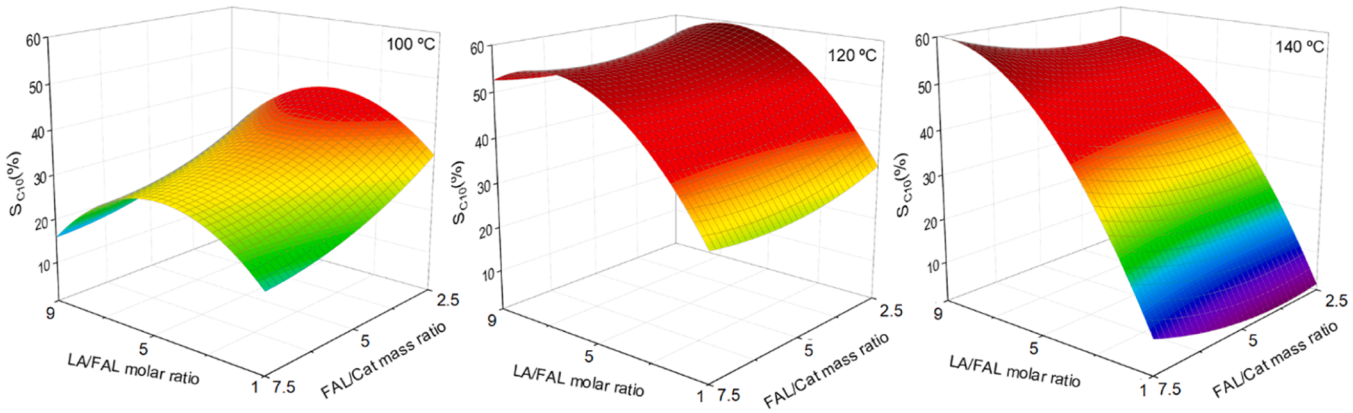

Fig. 5. Response surfaces corresponding to selectivity to C10 in the aldol condensation of FAL and LA over Zr-USY-2 predicted by the model at different temperatures.

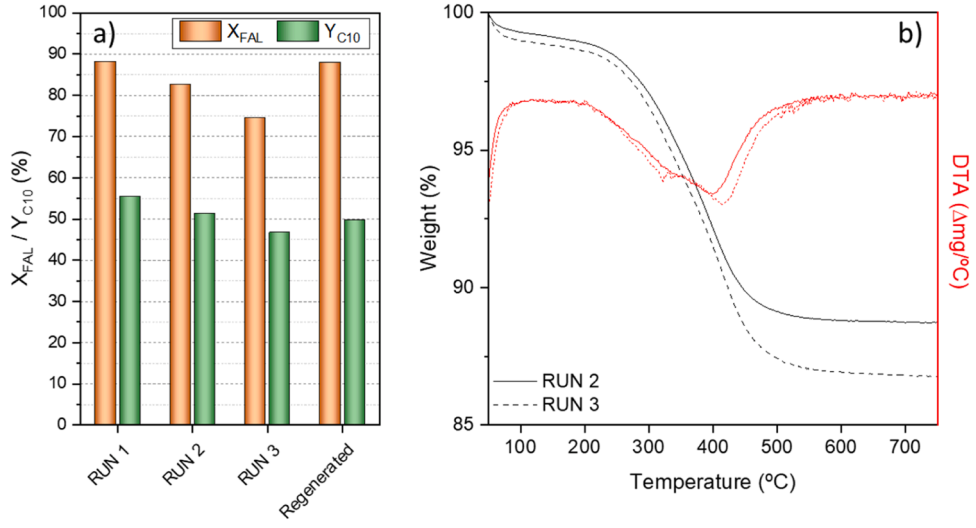

Fig. 6. a) Reusability of the Zr-USY-2 for the aldol condensation of FAL and LA. Reaction conditions: 2 h, LA/FAL = 9, T = 140 °C and FAL/CAT = 7.5. b) TGA analyses of the spent catalysts after run 2 and run 3.

was regenerated via calcination in air at 550 °C for 6 h. This process effectively removed the strongly adsorbed organic compounds that hinder the accessibility of the reagents to the active sites. As can be seen in Fig. 6a, the initial catalytic activity was almost fully restored, achieving the same FAL conversion and nearly identical C10 yield as observed in the first cycle. Therefore, the fouling of the catalyst surface is reversible through this thermal treatment.

4. Conclusions

The use of Zr-modified USY zeolites in the aldol condensation reaction between furfural and levulinic acid improves the activity and selectivity towards C10 oxygenated adducts as compared with the commercial parent USY zeolite. The acidity of the H-USY zeolite can be modulated by dealumination and subsequent incorporation of Zr in the structure, reducing the ratio of Brønsted/Lewis acid sites, which promotes condensation reactions over FAL polymerization reactions. By optimizing the reaction conditions for Zr-USY-2 catalyst, FAL conversions and yields to C10 can be increased from 55 % and 29 % to 88 % and 55 %, respectively, achieved at LA/FAL = 9 molar ratio and 140 °C after 2 h of reaction time. Catalyst reusability experiments indicate a small deactivation coming from surface fouling. However, thermal regeneration can fully restore the starting catalytic activity, confirming its stability. To the best of our knowledge, this work is the first one to prove the solvent-free aldol condensation of FAL and LA, achieving catalytic results comparable to those obtained in the aqueous phase under acid catalysis and avoiding neutralization steps during the procedure.

CRediT authorship contribution statement

Melero Juan A.: Writing – review & editing, Visualization, Validation, Supervision, Resources, Project administration, Funding acquisition, Data curation, Conceptualization. **Morales Gabriel:** Writing – review & editing, Validation, Supervision, Project administration, Funding acquisition, Data curation, Conceptualization. **Paniagua Marta:** Writing – review & editing, Validation, Supervision, Methodology, Data curation, Conceptualization. **Uzquiano Victor:** Investigation. **Uricochea Natalia:** Writing – original draft, Methodology, Investigation, Data curation.

Declaration of Competing Interest

The authors declare the following financial interests/personal relationships which may be considered as potential competing interests: JUAN ANTONIO MELERO reports financial support was provided by Spanish Ministry of Science and Innovation. If there are other authors, they declare that they have no known competing financial interests or

personal relationships that could have appeared to influence the work reported in this paper.

Acknowledgements

Financial support from the Spanish Ministry of Science and Innovation, through the project SAFADCAT (PID2021-122334OB-I00) is gratefully acknowledged.

Appendix A. Supporting information

Supplementary data associated with this article can be found in the online version at doi:10.1016/j.cattod.2025.115211.

Data availability

Data will be made available on request.

References

[1] J.I.C. Lau, Y.S. Wang, T. Ang, J.C.F. Seo, S.N.B.A. Khadaroo, J.J. Chew, A. Ng Kay Lup, J. Sunarso, Emerging technologies, policies and challenges toward implementing sustainable aviation fuel (SAF), Biomass. Bioenergy 186 (2024) 107277, https://doi.org/10.1016/J.BIOMBIOE.2024.107277.

[2] D.S. Lee, D.W. Fahey, A. Skowron, M.R. Allen, U. Burkhardt, Q. Chen, S.J. Doherty, S. Freeman, P.M. Forster, J. Fuglestvedt, A. Gettelman, R.R. De León, L.L. Lim, M. T. Lund, R.J. Millar, B. Owen, J.E. Penner, G. Pitari, M.J. Prather, R. Sausen, L. J. Wilcox, The contribution of global aviation to anthropogenic climate forcing for 2000 to 2018, Atmos. Environ. 244 (2021) 117834, https://doi.org/10.1016/J.ATMOSENV.2020.117834.

[3] V. Undavalli, O.B. Gbadamosi Olatunde, R. Boylu, C. Wei, J. Haeker, J. Hamilton, B. Khandelwal, Recent advancements in sustainable aviation fuels, Prog. Aerosp. Sci. 136 (2023) 100876, https://doi.org/10.1016/J.PAEROSCI.2022.100876.

[4] P. Yan, H. Wang, Y. Liao, C. Wang, Zeolite catalysts for the valorization of biomass into platform compounds and biochemicals/biofuels: a review, Renew. Sustain. Energy Rev. 178 (2023) 113219, https://doi.org/10.1016/J.RSER.2023.113219.

[5] G. Li, R. Wang, J. Pang, A. Wang, N. Li, T. Zhang, Production of renewable hydrocarbon biofuels with lignocellulose and its derivatives over heterogeneous catalysts, Chem. Rev. 124 (2024) 2889–2954, https://doi.org/10.1021/ACS.CHEMREV.2C00756/ASSET/IMAGES/LARGE/CR2C00756_0046.JPEG.

[6] F.D. Pileidis, M.M. Titirici, Levulinic acid biorefineries: new challenges for efficient utilization of biomass, ChemSusChem 9 (2016) 562–582, https://doi.org/10.1002/CSSC.201501405.

[7] B. Girisuta, H.J. Heeres, Levulinic Acid from Biomass: Synthesis and Applications, (2017) 143–169. ⟨https://doi.org/10.1007/978-981-10-4172-3_5⟩.

[8] A. Pundir, M. Singh Thakur, S. Prakash, N. Kumari, N. Sharma, Z. He, S. Nam, S. Dhumal, K. Sharma, S. Saxena, S. Kumar, S.V. Deshmukh, M. Kumar, Furfural as a low-volume, high-value asset from agricultural residues: a review on production, agricultural applications and environmental sustainability, Heliyon 10 (2024) e35077, https://doi.org/10.1016/J.HELIYON.2024.E35077.

[9] R. Gérardy, D.P. Debecker, J. Estager, P. Luis, J.C.M. Monbaliu, Continuous flow upgrading of selected C2-C6platform chemicals derived from biomass, Chem. Rev. 120 (2020) 7219–7347, https://doi.org/10.1021/ACS.CHEMREV.9B00846/ASSET/IMAGES/LARGE/CR9B00846_0129.JPEG.

[10] C. Wang, X. Zhang, Q. Liu, Q. Zhang, L. Chen, L. Ma, A review of conversion of lignocellulose biomass to liquid transport fuels by integrated refining strategies, Fuel Process. Technol. 208 (2020) 106485, https://doi.org/10.1016/J.FUPROC.2020.106485.

[11] G. Liang, A. Wang, X. Zhao, N. Lei, T. Zhang, Selective aldol condensation of biomass-derived levulinic acid and furfural in aqueous-phase over MgO and ZnO, Green. Chem. 18 (2016) 3430–3438, https://doi.org/10.1039/C6GC00118A.

[12] A.S. Amarasekara, T.B. Singh, E. Larkin, M.A. Hasan, H.-J. Fan, NaOH catalyzed condensation reactions between levulinic acid and biomass derived furan-aldehydes in water, Ind. Crops Prod. 65 (2015) 546–549, https://doi.org/10.1016/J.INDCROP.2014.10.005.

[13] M. Su, W. Li, Q. Ma, S. Li, T. Yang, X. Dou, Efficient synthesis of liquid fuel intermediates from furfural and levulinic acid via aldol condensation over hierarchical mfi zeolite catalyst, Energy Fuels 33 (2019) 12518–12526, https://doi.org/10.1021/ACS.ENERGYFUELS.9B03307/ASSET/IMAGES/LARGE/EF9B03307_0004.JPEG.

[14] L. Chen, Y. Liu, X. Zhang, J. Liu, Q. Zhang, L. Ma, Catalytic production of long-chain hydrocarbons suitable for aviation turbine fuel from biomass-derived levulinic acid and furfural, Fuel 334 (2023) 126665, https://doi.org/10.1016/J.FUEL.2022.126665.

[15] Y. Liu, L. Chen, Y. Chen, X. Zhang, J. Liu, Q. Liu, Y. Li, C. Wang, Q. Zhang, L. Ma, Pilot study on production of aviation fuel from catalytic conversion of corn stover, Bioresour. Technol. 372 (2023) 128653, https://doi.org/10.1016/J.BIORTECH.2023.128653.

[16] J. He, Q. Qiang, S. Liu, K. Song, X. Zhou, J. Guo, B. Zhang, C. Li, Upgrading of biomass-derived furanic compounds into high-quality fuels involving aldol condensation strategy, Fuel 306 (2021) 121765, https://doi.org/10.1016/J.FUEL.2021.121765.

[17] J. Cueto, V. Korobka, L. Faba, E. Diáz, S. Ordóñez, Aldol condensation of biomass-derived levulinic acid and furfural over acid zeolites, ACS Sustain Chem. Eng. 8 (2020) 4371–4383, https://doi.org/10.1021/ACSSUSCHEMENG.9B06636/ASSET/IMAGES/LARGE/SC9B06636_0010.JPEG.

[18] J. Cueto, L. Faba, E. Díaz, S. Ordóñez, From lignocellulosic biomass to chemical precursors: simultaneous valorization of furfural and levulinic acid over mesoporous acid catalysts, Ind. Crops Prod. 188 (2022) 115692, https://doi.org/10.1016/J.INDCROP.2022.115692.

[19] C. López-Aguado, M. Paniagua, J. Iglesias, G. Morales, J.L. García-Fierro, J. A. Melero, Zr-USY zeolite: efficient catalyst for the transformation of xylose into bio-products, Catal. Today 304 (2018) 80–88, https://doi.org/10.1016/J.CATTOD.2017.08.031.

[20] V. Zholobenko, C. Freitas, M. Jendrlin, P. Bazin, A. Travert, F. Thibault-Starzyk, Probing the acid sites of zeolites with pyridine: quantitative AGIR measurements of the molar absorption coefficients, J. Catal. 385 (2020) 52–60, https://doi.org/10.1016/J.JCAT.2020.03.003.

[21] J.T. Scanlon, D.E. Willis, Calculation of flame ionization detector relative response factors using the effective carbon number concept, J. Chromatogr. Sci. 23 (1985) 333–340, https://doi.org/10.1093/CHROMSCI/23.8.333.

[22] T. Barzetti, E. Selli, D. Moscotti, L. Forni, Pyridine and ammonia as probes for FTIR analysis of solid acid catalysts, J. Chem. Soc. Faraday Trans. 92 (1996) 1401–1407, https://doi.org/10.1039/FT9969201401.